Journal of Computers Vol. 30 No. 2, 2019, pp. 126-134
doi:10.3966/199115992019043002011

Analysis from Image Processing of Wildfire Area for a Long-Term Protection Plan

Ekkarat Boonchieng[1], Varin Chouvatut[1,2*]

[1] Center of Excellence in Community Health Informatics, The Theoretical and Empirical Research Group

[2] Department of Computer Science, Faculty of Science, Chiang Mai University, Chiang Mai, Thailand
ekkarat@boonchieng.net, varinchouv@gmail.com

Received 15 December 2018; Revised 15 February 2019; Accepted 15 February 2019

Abstract. This research involves the implementation of a system that interprets the burnt area obtained from satellite imagery, displaying an image showing the burnt area from satellite imagery, and processing online through a website. This proposed method processes the interpretation based on image processing techniques applied to satellite images. It does not follow the usual process of using heat sensors (or temperature sensors). There are major disadvantages with the use of heat sensors including a large budget required in setting up the sensors and uncertainty about how far an infrared temperature sensor can measure. For the infrared sensor, the D to S ratio may be used to answer the question where D is the distance between the sensor and the target to be measured and S is the diameter of the area measured from the sensors on which the heat temperature touches the sensors' detection surface. This paper aims to manage this problem of using sensors by satellite image processing.

Keywords: burn scar, heat sensor, infrared, satellite imagery

1 Introduction

There recently have been many wildfires in Chiang Mai a province in northern Thailand, due to various reasons. They usually take place during the late rainy season through the early winter, which leads to agricultural benefits and maybe some other factors.

Officers in the Chiang Mai province now pursue a policy and a plan to prevent and alleviate this difficult situation. One way to achieve their goal is to monitor and analyze the region of a forest which is being burnt or which was burnt. While the former case is recently unavailable, the latter can be done through satellite imagery. Satelite imagery can now be observed directly by eyesight and then analyzed. However, with the aid of a computer, there would be positive improvements on both processing speed and accuracy.

We, therefore have made a processing system that can be used to interpret the burnt area captured from satellite imagery and display the captured area process online through a website. This is a very effective and practical new implementation.

In the past, all the processes have been implemented using only satellite-image processing without the use of costly heat sensors.

2 System in Details

In this section, details of how a digital image can be obtained finally and how our system works will be described in sections including Sect. 2.1 explains how raw data can be acquired from a satellite; Sect. 2.2 explains how the analog signal can be converted into the digital one; Sect. 2.3 explains an important

* Corresponding Author

feature of the digital image which is data resolution; and Sect. 2.4 explains how boundary of a wildfire area can be detected according to our aim.

2.1 Data from Satellite Imagery

In the data measurement using remote measurement equipment, the equipment would record data in terms of radiation level or radiation intensity in each spectrum of the instantaneous field of view (IFOV) [1, 3, 5]. The data recorded into two formats [2]:

Analog data. This format of continuous data, in the form of radiation intensity, is recorded by the measurement equipment. This way of recording results in gaining continuous measured data, such as light intensity [9] that appeared in satellite images which are recorded on an aerial sensitive film [10] as illustrated in Fig. 1(a).

Digital data. This data format recorded by the measurement equipment used in [8] is obtained discretely by the way that the measurement equipment would convert the input analog (continuous) data [9] into their nearest integers in the range determined in the system. Thus, output data resulting from such conversion are discontinuous, unlike the originally recorded data which are continuous. The differences in values resulting from conversion are similar to stair steps, each step is known as an intensity level. The process used to acquire these discrete intensity levels is called quantization and the digital data, in terms of radiance, which are quantized into discrete levels are called quantized radiance. An example of the quantized radiance converted from analog data as Fig. 1(a) is Fig. 1(b).

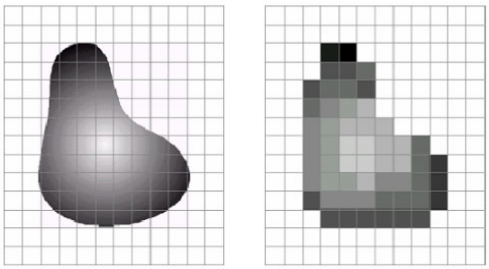

(a) analog data (b) digital data

Fig. 1. Example of the two formats of recorded data [5]

The measurement equipment recorded that the 8-bit data is capable of storing data levels in the range of 0 to 255 separately as expressed in Fig. 2. Data representing radiance intensities after quantization would be digitally stored using n bits for storing 2n intensity levels. Typically, the numerical data will be quantized into 256 levels, thus, can be called 8-bit data.

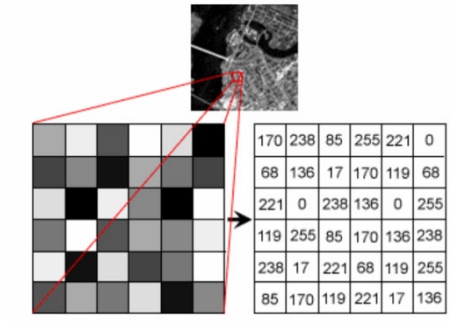

Fig. 2. Example of 8-bit numerical data which can store gray levels of up to 256 levels [5]

In this way, if the measurement equipment [9] is designed with the capability of recording with more details and higher levels of radiation intensity, the measured data will provide more continuous (or narrower) radiation intensity levels. Meanwhile, the amount of recorded data will be increased unavoidably. Fig. 3 shows the graphical data with different intensity levels; Fig. 3(a) is represented by 16 intensity levels, Fig. 3(b) eight levels, Fig. 3(c) four levels, and Fig. 3(d) two levels.

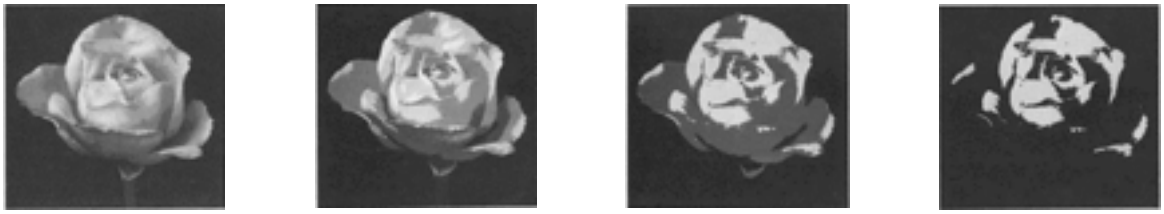

(a) 16 intensity levels (b) Eight levels (c) Four levels (d) Two levels

Fig. 3. Example of a graphical data represented [4]

2.2 Conversion from an Analog Image to its Numerical Representation

The light amount recorded by a sensing receiver together with the quantitative measurement from a densitometric unit will be converted into numerical brightness (or an intensity level), BVi,j,k representing the brightness value at the position of row i and column j for spectral band k. At the end of a scanline, the sensing receiver will move its position down the y-axis for one unit and after that it will scan along the line parallel to the previously scanned line. Once the whole image was completely scanned, a numerical representation of the image whose basic components are points or pixels is thus obtained. The conversion from an analog signal of a satellite image to its corresponding numerical representation results in a matrix of brightness intensities recorded in the format of 8-bit data where range of the brightness is between 0 and 255 levels. This matrix form of the data will be stored and backed up as shown in Fig. 4 for further numerical analysis [4].

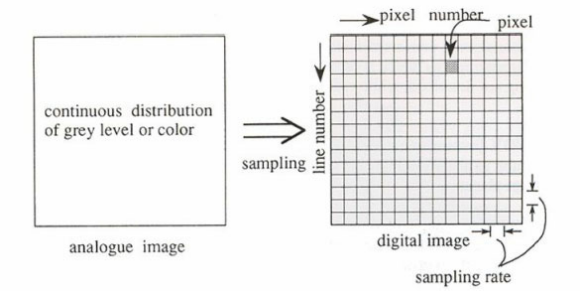

Fig. 4. Conversion from the analog signal of a satellite image to its corresponding numerical matrix

For the pixel ground resolution obtained from the satellite imagery, there will be ratios of aerial images with respect to the instantaneous field of view (IFOV), which was used for the scan.

The scanned resolution is usually measured in the units of dots per inch (dpi) and micrometers (μm). Thus the pixel ground resolution can be computed from (1) and (2).

(1) In the unit of dots per inch,

$$(\text{dpi})\ PM = (S / \text{dpi}) / 39.37; \quad \textbf{(1)}$$

(2) In the unit of micrometers,

$$(\mu\text{m})\ PM = (S \times \mu\text{m}) \times 0.000001; \quad \textbf{(2)}$$

where: PM = size of pixel or dot in the image
S = ratio of the image obtained from satellite imagery.

2.3 Resolution of the Numerical Data

According to the information of ERDAS, which is a remote sensing application [7], digital image resolutions in remote sensing can be categorized into four types

Spectral resolution. This resolution is a specific spectrum in the electromagnetic spectrum [1], which the measurement equipment can detect and record. In the visible bands of spectrum, any wide range of spectrum indicates a rough spectral resolution while any narrow-ranged spectrum indicates a fine spectral

resolution. For example, the first detectable spectrum of the measurement equipment of the Landsat satellite with Thematic Mapper (TM) system will be able to record a spectral power in the range of 0.45-0.52 micrometers. The panchromatic measurement equipment of the SPOT satellite can detect and record electromagnetic spectrums whose wavelength is between 0.51-0.73 micrometers. Such range of the wavelengths is called a rough spectral resolution (a wide range) comparing with the third spectrum of the Landsat-TM satellite, which can detect and record spectrums whose wavelength is between 0.63-0.69 micrometers. The latter range of spectrums is called a fine spectral resolution (a narrow range). Fig. 5 illustrates spectral resolutions for different spectral bands such as explained in [11].

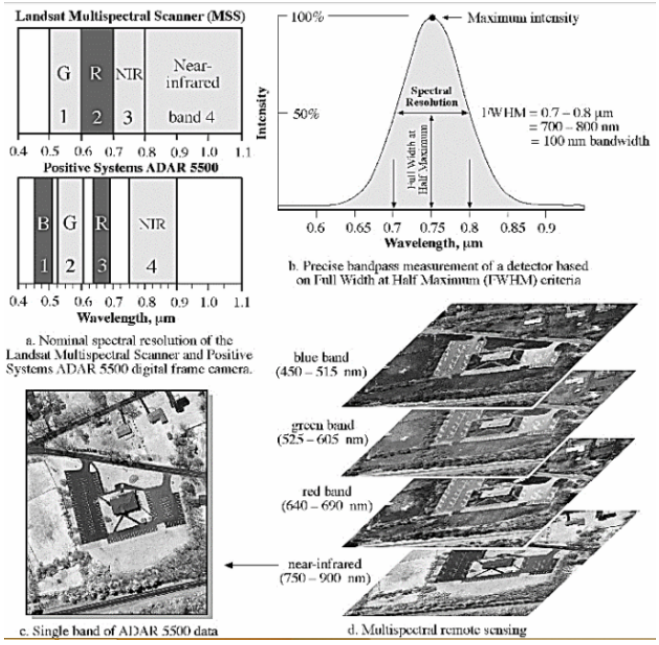

Fig. 5. Example of the spectral resolutions of various spectral bands [5]

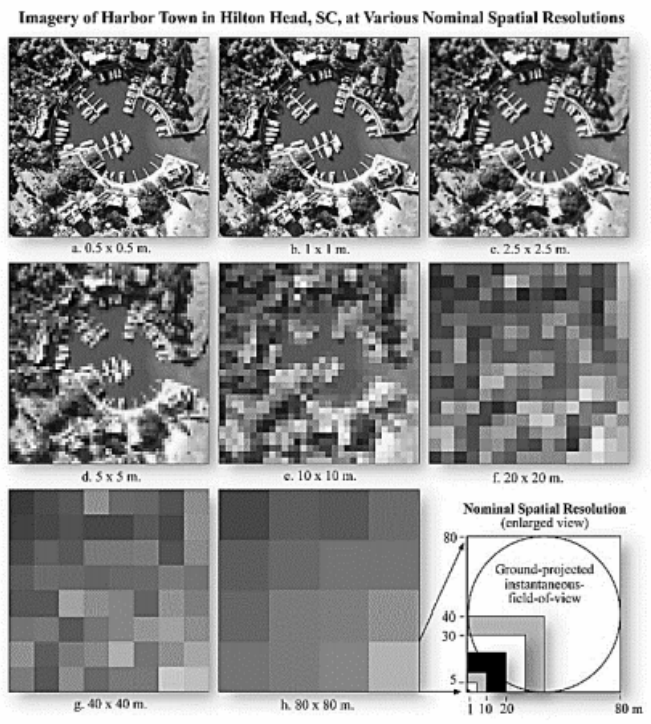

Fig. 6. Illustrative example of different spatial resolutions [5]

Spatial resolution. The spatial resolution can be represented by the smallest object, which still can be separated by measurement equipment [6, 15]. The scale of an image is the ratio of distance on the image to the real distance on the ground. The ability in displaying a ground region in each image point can also be used to represent the spatial resolution. A larger number of spatial resolutions means a lower resolution than a smaller number of spatial resolutions. For example, a spatial resolution of 89 meters will provide rougher images than a spatial resolution of 9 meters. This is because the spatial resolution has a direct relationship with an image's scale. But the term scale in remote sensing, is defined by an image whose points display a small size of a ground region. For example, the data from SPOT has a spatial resolution of 10 or 20 meters. On the other hand, a small scale means an image whose points are used to display a large region of the ground, as shown by the data from NOAA-AVHRR with a spatial resolution of 1.1 kilometers. Fig. 6 shows the direct relationship between the spatial resolution [12-13] and the instantaneous field of view (IFOV) whose measured unit is in radian at the time data are recorded by the measurement equipment. The relationship between the spatial resolution and the IFOV is as (3).

$$d = 2 \times H \times \tan (IFOV / 2) \quad \textbf{(3)}$$

where: d = the ground distance per one information unit (an image point)
H = height of the observation position
IFOV = the instantaneous field of view

Radiometric resolution. Radiometric resolution is a dynamic range or the number of possible data for each spectrum recorded in image files. This resolution can be indicated using the number of bits representing a ray's power which can be divided and recorded into individual components. For example, 8-bit data has a range of values between 0 to 255. This radiometric resolution is more important in numerical analysis than in visual analysis. The gray levels or intensity levels of visible rays that a human can distinguish are not more than 64 levels and thus those indistinguishable by a human's eyesight are over 200,000 levels. Consequently, 246 levels of each spectrum are surely too many for a human's eyesight. However, numerical analysis of an image processed by a computer using all available radiometric resolutions, not just 246 levels, helps in distinguishing objects with similar spectral signature correctly as Fig. 7.

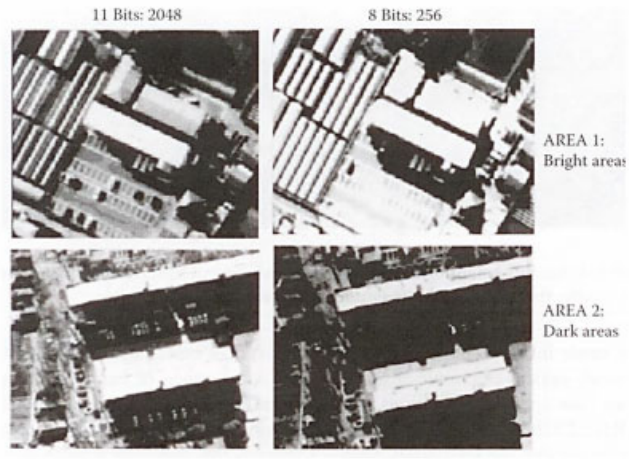

Fig. 7. Radiometric resolution helps in distinguishing objects with similar spectral signatures [5]

Temporal resolution. This kind of resolution is the ability in repeatedly capturing images of the measurement equipment on the same ground area. For example, the Landsat satellite can capture images of the same areas around the whole world repeatedly every 16 days while the SPOT satellite can capture images of the same areas repeatedly every 26 days. Fig. 8 shows an illustration displaying examples of temporal resolution.

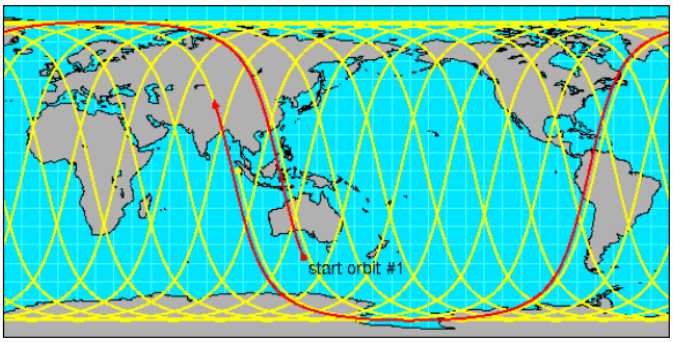

Fig. 8. An illustrative example of repeated capture of a satellite traversing around the world [5]

2.4 Processing Steps

To extract or detect the boundary of a wildfire area, the following steps are done.

Image filtering. Filtering images means to pass a signal filter through an input image and thus provide the output image, which has different features from the input. The major purpose of image filtering is to enhance or attenuate some features of an image in order to gain a required property of the image.

Convolution filtering. Most filtering techniques are based on average computation, which may be an average of the same point on several images or may be an average of points surrounding a point of interest.

The average computation is an attenuated filtering and most filtering techniques are suitable for reducing noise. These are kinds of signals which involve high frequency. As mentioned before, an enhanced filtering technique aims to augment some required features in the image while an attenuated filtering technique aims to attenuate some unwanted features in the image.

We cannot use average computation if we want to emphasize the changing of points in an image, which is similar to filtering an image using a high-pass filter, Instead, in this case, we can use the convolution technique.

In image processing, convolution is a method computing between a template and a target image. Template is a matrix with dimensions of n × m composed of a set of numerical elements to be superimposed with corresponding elements of the input image to calculate the convolution results. Let template T(x, y) be a template with dimensions of n × m and image I(X, Y) have dimensions of N × M. The convolution, I'(X, Y), between template T and image I can be found from (4):

$$I'(X, Y) = T(x, y) \times I(X, Y) = \Sigma i \, \Sigma j \, \{ \, T(i, j) \times I(X - i, Y - j) \, \}; \quad \textbf{(4)}$$

where i = 0..(n-1) and j = 0..(m-1).

Edge detection. Edge detection is finding an object's boundary in an image. Once the edge of the boundary around the target object has been found, the area of the object may be calculated or even an object recognition may be achieved. However, searching for a complete and precise edge of an object is not that easy, especially, when the edge of the object appeared in the image is of low quality, e.g. the difference between foreground and the background is not obvious or the overall brightness of the image is uncertain. This incompleteness of edges is mainly because an edge in image is caused by the difference of intensity from one point to another thus if this level of difference is high, the edge appeared in the image will be obvious but if this difference level is low, the appeared edge may be blurred.

A simple method to find a horizontal edge is to find differences between a point and its lower (or upper) point. That is,

$$Ydiff(x, y) = I(x, y) - I(x, y+1) \quad \textbf{(5)}$$

where Ydiff = different value in vertical axis
I(x, y) = intensity of the point at position (x, y).

To find a vertical edge, the similar technique as used in (5) can be used but change the x component to y component instead. Thus, it is to find differences between a point and its left (or right) point.

Sometimes, we may want to find the result of combining both horizontal and vertical differences together to measure the gradient magnitude of the edge.

We will apply its absolute value or squared value in each direction to prevent the plus and minus signs of the direction of the gradient vector.

Other than finding the magnitude of the gradient vector, the vector's directions is also useful. The process of finding the gradient vector's direction can be done using formula (6) below.

$$GD(x, y) = \arctan \{ Ydiff(x, y) / Xdiff(x, y) \} \quad \textbf{(6)}$$

where GD(x, y) = direction of the edge at position (x, y).

3 Experimental Results

From the obtained images by satellite imagery, an example result of segmentation [14] of the burnt area in a forest is as shown in Fig. 9 to Fig. 12.

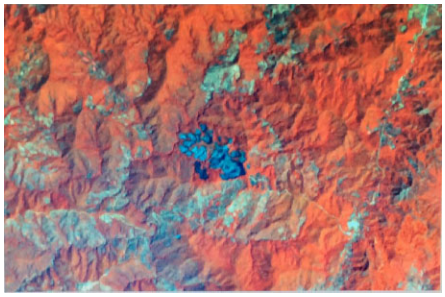

Fig. 9. The obtained satellite image showing burnt areas in a forest

From Fig. 9, the burnt areas of the forest are displayed as dark blue dots. This image will be further processed as separate layers based on the different components of light colors and then segment the target areas.

Fig. 10. The image resulted from layer separation

Fig. 10 shows the resulting image obtained after the process of segmentation.

Fig. 11. Result image after background subtraction

After segmentation, the background of the image should be filtered out using the background subtraction technique. The results from the background subtraction is shown in Fig. 11. The next step

requires the background-subtracted areas to be superimposed with the original satellite image, Fig. 9, and thus the resulting image is shown in Fig. 12.

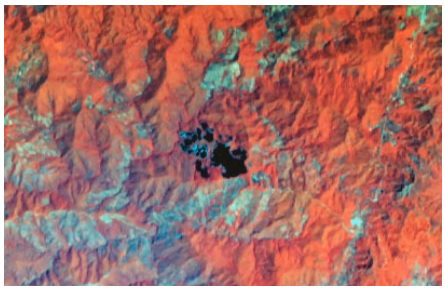

Fig. 12. Result image showing burnt areas superimposed with the satellite image from Fig. 9

4 Conclusion

The graphical results showed us that the images from the satellites can be analyzed numerically using layer separation, background subtraction, burnt area segmentation, and superimposition. The obtained graphical results can then be used in a higher level of analysis, which involves, counting the number of burnt areas and finding the size of the finer burnt areas.

Acknowledgements

Input data from this paper are provided by The Center of Excellence in Community Health Informatics (COEiCHI), Chiang Mai University, Thailand. Collection of real data is from an online application developed by COEiCHI.

References

[1] S. Hiranvarodom, Modeling of strategy for photovoltaic development and dissemination in Thailand, in: Proc. 2003 3rd World Conference on Photovoltaic Energy Conversion, 2003.

[2] T. Tossanon, Digital image analysis and interpretation, [dissertation] Suranaree University of Technology, 2007.

[3] S. Ongsomwang, Principles of remote sensing and digital image processing, [dissertation] Nakhon Ratchasima Province, Thailand: Suranaree University of Technology, 2011.

[4] J. R. Jensen, Introductory Digital Image Processing: A Remote Sensing Perspective, third ed., Practice Hall, 2005.

[5] J. R. Jensen, Remote Sensing of the Environment: An Earth Resource Perspective, second ed., Practice Hall, 2007.

[6] Teaching (240-373). <http://fivedots.coe.psu.ac.th/~montri/Teaching/240-373/>, 2017 (accessed 10.12.17).

[7] ERDAS IMAGINE. <http://www.hexagongeospatial.com/products/power-portfolio/erdas-imagine>, 2018 (accessed 17.01.18).

[8] M. Kovac, Efficient data compression algorithm for data loggers, measurement equipment and remote data analysis applications, in: Proc. 1998 IEEE Proceedings of Southeastcon, 1998.

[9] R.O. Lane, T.A. Badran, G.F. Marshall, Measurements for remote identification of electrical equipment, IET Electronics Letters 53(15)(2017) 1001-1005.

[10] L.W. Ming, L. Xue, Ch. X. Hui, L.Q. Jun, Development situation and trend of domestic and international aerial mapping camera, in: Proc. 2011 International Conference on Mechatronic Science, Electronic Engineering and Computer (MEC), 2011.

[11] M. Albughdadi, D. Kouame, G. Rieu, J.-Y. tourneret, Missing data reconstruction and anomaly detection in crop development using agronomic indicators derived from multispectral satellite images, in: Proc. 2017 IEEE International Geoscience and Remote Sensing Symposium (IGARSS), 2017.

[12] Sh. V. Naidu, A. Garg, H. Yahia, Dh. Singh, A comparison of wavelet based techniques for resolution enhancement of moderate resolution satellite images, in: Proc. 2015 National Conference on Recent Advances in Electronics & Computer Engineering (RAECE), 2015.

[13] K. S. Shamna, Satellite image resolution and brightness enhancement using discrete, stationary wavelet and singular value decomposition, in: Proc. 2014 International Conference on Power Signals Control and Computations (EPSCICON), 2014.

[14] Y. Zhang, L. Chen, Z. Zhao, J. Jia, HuaMulti-focus image fusion based on image decomposition and quad tree decomposition, Journal of Computers 25(3)(2014) 1-10.

[15] X.-H. Zeng, S.-L. Hou, Manifold-regularization super-resolution image reconstruction, Journal of Computers 28(1)(2017) 119-136.